Jurnal Polimesin
Department of Mechanical Engineering
State Polytechnic of Lhokseumawe
http://e-jurnal.pnl.ac.id/polimesin
e-ISSN : 2549-1999 No. : 6 Month : December
p-ISSN : 1693-5462 Volume : 22 Year : 2024

Article Processing Dates: Received on 2024-06-28, Reviewed on 2024-11-28, Revised on 2024-12-12, Accepted on 2024-12-15 and Available online on 2024-12-30

Hydroxyapatite-reinforced Al-Mg composites for corrosion resistance in hanks' balanced salt solution

Zuliantoni[1,*], W. Suprapto[2], P.H. Setyarini[2], F. Gapsari[2]
[1]Mechanical Engineering Department, Bengkulu University, Bengkulu, 38371, Indonesia
[2]Mechanical Engineering Department, Brawijaya University, Malang, 65145, Indonesia
*Corresponding author: zuliantoni@unib.ac.id

Abstract

Aluminum-Magnesium (Al-Mg) matrix composites were fabricated using powder metallurgy. Ceramic particles such as synthetic hydroxyapatite and snail shell hydroxyapatite were used as reinforcing particles. Snail shell hydroxyapatite often shows superior corrosion resistance over manufactured hydroxyapatite because of its distinct structural integrity, biological compatibility, and trace element concentration. Aluminum-magnesium matrix composites are lightweight metals with advantageous mechanical, physical, and density properties, making them suitable for applications in the automotive, aerospace, biomedical, and sports industries. However, their limited corrosion resistance has restricted their broader development and application. This study characterizes corrosion behavior of Al-Mg composites reinforced with HAss and HA bioceramic. Given that plastic deformation can improve corrosion resistance, powder metallurgy is one of the most promising techniques for improving a material's mechanical properties. Following HAss reinforcement testing, Al-Mg composites were contrasted. A compression pressure of 650 MPa was used to produce the samples at room temperature. Corrosion was measured using the potentiodynamic polarization electrochemical test in Hank's Balanced Salt Solution (HBSS). Out of all the Al-Mg/HAss composites, the 0.55Al-0.05Mg/0.40HAss composite exhibited the maximum corrosion resistance (9.58×10^{-4} mmpy), per the test results. 7.72×10^{-6} mmpy was the Al-Mg/HA composite's ideal corrosion resistance when combined with the 0.80Al-0.05Mg/0.15HA composite. The application of powder metallurgy in the production of the composites significantly improved their corrosion resistance. The Al-Mg/HAss AMC can also be used in biomaterials.

Keywords:
Composite Al-Mg, hydroxyapatite, powder metallurgy, corrosion rate, HBSS.

1 Introduction

Most of the work on Metal Matrix Composites (MMC) is based on Al. Light metals and their alloys, such as those made of magnesium and aluminum, have excellent strength-to-weight ratios and low densities [1]. Magnesium has recently acquired popularity as a metal that may be used as a matrix because it is two to three times stronger than aluminum [2]. The usage of the light metals Al and Mg may be very beneficial for future energy-saving projects in many different industries, including manufacturing, building, power generation, transportation, and many more. Al and Mg are commonly combined for increased strength, weldability, and corrosion resistance [3]. The potential for Aluminum-metal Matrix Composites (AMC) to replace traditional alloys is high because of their low weight and simplicity of manufacturing [4]. Recent studies have shown that aluminum alloys can be considerably strengthened by increasing the size of the steel [5].

This study presents snail shell hydroxyapatite (Hass) as a novel, environmentally friendly reinforcement for Al-Mg matrix composites, providing enhanced corrosion resistance because of its inherent structural benefits and bioactive qualities. A further layer of innovation in the search for materials with improved corrosion resistance is added by the use of powder metallurgy to create these composites at room temperature under compression pressure. Aluminum alloys are widely used in warships and offshore constructions due to their higher strength, durability, weldability, and resistance to corrosion [6].

Magnesium solid solution strengthening increases the strength of the Al-Mg alloy. Magnesium atoms take the role of Al and form a spherical stress field around the dissolved atoms. The moving dislocations interact with the stress field and generate elastic interaction energy due to the differences in size and modulus between the Al matrix and the dissolved magnesium atoms. It has been demonstrated that magnesium concentrations in Al alloys up to around 5% weight percent remain in a solid solution, greatly enhancing strength and toughness while avoiding stress corrosion cracking [7]. Al and Mg typically have electrode potentials of 1.676 V and 2.356 V, respectively. These possible differences cause Al-Mg compounds to have low hardness, poor wear resistance, and a high risk of galvanic corrosion. The use and promotion of Al-Mg compounds are therefore promoted [8].

It is difficult to choose reinforcement that increases the corrosion resistance of solidified AMC since different reinforcement particles have a direct impact on the corrosion properties of the generated AMC [9]. Even though synthetic Hydroxyapatite (HA) is extensively researched and utilized in medical implants, there are still issues with its brittleness and low corrosion rate in some applications. However, because of its natural source and promise for a more environmentally friendly method, HAss presents an intriguing substitute. The mineral makeup of snail shells is identical to that of HA, making them more affordable, plentiful, and providing comparable mechanical and bioactive advantages [10]. It is anticipated that adding HA and HAss to Al-Mg composites will improve their corrosion resistance as well as their biological performance, especially for uses in the biomedical industry. In addition to providing further economic and environmental advantages, the natural and synthetic forms of hydroxyapatite work in tandem to reinforce the matrix. With an emphasis on enhancing the mechanical and bioactive qualities of Al-Mg composites, this work attempts to investigate the possibilities of these hydroxyapatite reinforcements [11]. Kaewdaeng and Nirunsin claim that HAss is used as a filler in several composite applications [12] and has a high CaO content [13].

It demonstrated that both HA and HAss increase the corrosion resistance of metals such as aluminum alloys. Because HA coatings are chemically stable and bioactive, they can serve as a barrier to keep corrosive substances from reacting with the underlying metal. Because of its comparable composition to synthetic HA, HAss also improves corrosion resistance by forming a protective layer. However, research indicates that natural HAss may have distinct microstructural properties that, when added to metallic matrices, could result in a more uniform or optimal protective layer [14]. Trace elements and contaminants found in snail shell HAss may improve its effectiveness under particular environmental circumstances. By encouraging passivation and lowering the chance of localized corrosion, the natural composition of HAss, for instance, may provide extra ionic exchange qualities that could enhance the Mg composite's resistance to corrosion [15].

Synthetic HA and HAss are expected to enhance the mechanical and biological performance of Al-Mg composites, particularly for applications in the biomedical sector. This shell is a byproduct that is thrown away once the contents have been extracted. The most common inorganic filler in polymers is calcium carbonate precipitate ($CaCO_3$) [16]. $CaCO_3$ is one example of a ceramic reinforcing particle with

remarkable functional properties. Ceramic reinforcement is structurally useful and has been shown to be a potential strengthening material at high temperatures due to its exceptional properties, which include good corrosion resistance, high thermal conductivity, high stiffness, good chemical resistance, good electrical conductivity, good wear resistance, high hardness, low density, high melting point, and high elastic modulus [17]. It has been demonstrated [18] that adding calcium carbonate-containing snail shells to composite materials for concrete and polymers improves their qualities [19].

Based on the results of a review of previous studies, this study uses HAss as reinforcement to increase the corrosion resistance of Al-Mg AMC and then compares it with HAss reinforcement. The HA in question is synthetic HA, which is available for purchase. The primary components utilized to create synthetic hemophilus are calcium carbonate, calcium hydroxide, calcium nitrate, diammonium hydrogen phosphate, and ammonium hydroxide. Usually, sticks and balls are the only types of synthetic HA. The cost of synthetic HA is higher than that of natural HA. Synthetic HA is quite expensive because it is made with extremely pure chemicals. Natural hydroxyapatite materials come from plants, algae, minerals, shells, water, the sea, and mammals [20]. To reduce costs, abundant snail shell debris was substituted for HA. Over the past few decades, a lot of research has been done on the synthesis of bioceramics from biological waste materials, such as snail shells [21].

Natural hydroxyapatite has excellent bioactive and crystallographic qualities and produces numerous layers of apatite [22]. Because of its bioactive properties, apatite deposition can happen spontaneously. By using a protective layer that contains apatite, corrosion can be prevented [23]. Natural hydroxyapatite might provide an alternate biomaterial in the realm of biomedical engineering. Bioceramic reinforcements, such as HA, can be used since they are structurally and compositionally identical to real bone. HA is also biocompatible and osteoconductive [24]. It is possible to split waste snail shells into HA particles and use them as an AMC reinforcement. Therefore, it is essential to conduct research on natural HA as an AMC material to replace synthetic HA.

Numerous methods, including casting [25] and Powder Metallurgy (PM) [26], can be used to create AMC. Of these production methods, PM is the most attractive due to its uniform reinforcing distribution, finer grain structure, and superior mechanical characteristics. High sintering temperatures increase hardness [27]. Additionally, the PM process avoids chemical reactions between the reinforcement and matrix by operating at a lower temperature than casting. In the first step of the process, high-dispersion composite powder is made, and in the second step, it is compacted. One strategy for enhancing corrosion resistance is MMC [28].

Lightweight Al-Mg alloys with advantageous mechanical and thermal properties can be used as an MMC matrix [29]. Most of the aluminum in the Al-Mg alloy is in solid solution, and it has a melting point of roughly 650°C. One of the precipitates is the intermetallic complex β-$Mg_{17}Al_{12}$ (β phase), which is electrochemically cathodic to the α-Mg matrix. An alloy's corrosion is influenced by its volume fraction, particle size, and distribution. The corrosion behavior of the composite is affected by the type of reinforcement. The findings of the immersion show that the increase in corrosion rate brought on by the area of reinforcement is a major factor affecting the corrosion process of silicon carbide-reinforced composites. In their study of the corrosion behavior of aluminum-silicon alloy matrix composites reinforced with different mass concentrations of Al_2O_3 particles, Saber et al. were able to achieve greater corrosion resistance by increasing the mass percentage of Al_2O_3 reinforcement [30].

PM in NaCl or Hanks' Balanced Salt Solutions (HBSS) are frequently used in electrochemical characterizations of magnesium [31]. Several different chemical reactions may occur when different ions are added to the NaCl solution in HBSS. With a higher chloride content, HBSS is a more aggressive medium. Sulfate ions in HBSS can cause higher corrosion rates when magnesium and its alloys are compared to other corrosion media that are used to characterize the corrosion properties of materials [32]. The corrosion product layer is rapidly broken down in conditions such as saltwater that contains chlorine ions [33]. Among other types of corrosion, aluminum alloys experience pitting, intergranular, and scale corrosion in salt solutions [34]. Additionally, it is observed that chloride ions are attacking the electrolyte. This attack quickly weakens the passive layer that has formed on the sample surface, and the formation of secondary or intermetallic deposits exacerbates pitting corrosion. The precipitates that form at grain boundaries are susceptible to local corrosion [35].

Previous research showed that HA particles were used as MMC reinforcement. Jaiswal et al. investigated the corrosion behavior of Mg-3Zn-5HA compounds in SBF solutions prepared via powder metallurgy [36]. The results showed that the samples' resistance to corrosion was increased after being immersed for 56 days. However, the HA strengthening produced from natural materials, such as snail shell hydroxyapatite, which is used in AMC with different compositions, was not included in this work. Radha and Sreekanth investigated the mechanical properties and corrosion behavior of compression-molded MMC Mg-5HAp and Mg-1Sn/5HAp [37]. Test findings show that MMC Mg-1Sn/5HAp increases maximum compressive strength, yield strength, hardness, and corrosion resistance. It's unclear, nevertheless, if employing the powder metallurgy production method with HA-reinforced snail shell hydroxyapatite has an impact.

Aiello and Sieradzki then investigated Mg-Al binary alloys (Al = 2, 5, and 8%) that were annealed in He/Ar for six days at 425ºC and subsequently cooled by water to room temperature [38]. Simultaneously, synthetic alloys are also manufactured using photolithography processes. Thirty milliliters of 0.6 M NaCl solution were immersed for one minute and twenty hours to check for corrosion. The corrosion characterisation results show that as the amount of Al increases, so does the corrosion potential. The initial corrosion potential and the synthetic alloy with 5% Al behaved quite similarly at the same time; however, after a 20-hour soak, the synthetic alloy's corrosion potential increased from 0.11 V to 0.25 V. However, this work did not investigate the effect of HA particles as a reinforcement for Mg-Al MMC.

Choi et al. discuss grain size and corrosion current density in hot extrusion, cold rolling, and annealing The results showed that anodic deposits were more widely dispersed as fine grain size increased, which led to a decrease in the corrosion current density. Due to their non-homogeneous nucleation sites, which raise the volume % of anodic deposits, sensitized cold rolled samples yield the greatest results. However, whether adding HA affects powder metallurgy's capacity to generate MMC is still uncertain. Kim et al. [40] looked at the formation of precipitates with finer grain sizes when the Mg content in pure Al is increased from 5% by weight. Therefore, to achieve the ideal biomaterial composition, it appears that more research is required before adding HA particles to Al-Mg alloys.

Kim, Kang, and Lim [41] state that as the magnesium content rises, so do the alloy's elongation, yield strength, and fracture strength. The Al-7Mg alloy combination also produces the best durability and strength. However, it is not yet known if adding HA to these ingredients can enhance the results of powder metallurgical processes used to create MMCs. According to Pramono A. et al. [42], the combination of HA-Al-Mg in MMC produced utilizing the high-temperature synthesis technique has potential as a biomaterial. The study found that the composite samples of beef bone and cans with the composition 85HA-10Al-5Mg met the ASTMF138 standard for biomaterial elements due to their 30% porosity and 73 HV hardness. Therefore, it is interesting to examine how the corrosion of MMCs might be described using powder metallurgy approaches.

Google, PubMed, and Sciencedirect search keywords almost no research has been done on characterizing Al-Mg MMCs using powder metallurgical treatment of HAss reinforcing powder. In view of these results, this study recommends the use of an Al-Mg/HAss combination as a component of MMC. After that, the corrosion characterization of the Al-Mg/HAss MMC was evaluated. The powder metallurgy process is perfect for creating AMC Al-Mg/HAss since it can produce a good blend of metals and non-metals. Additionally, this strategy lessens the

disadvantages of segregation [43]. The results of this study are expected to be useful to the automotive, aerospace, and sports industries. It can also be used as a biomaterial in bone and dental implants. Thus, the goal of this study is to strengthen HAss in order to increase Al-Mg AMC's resistance to corrosion. After that, these outcomes were contrasted using AMC and HA reinforcement.

2 Methods

2.1 Materials and Tools

The study's selection of HA (both synthetic and natural HAss) offers a well-rounded strategy that maximizes mechanical qualities, corrosion resistance, and bioactivity without sacrificing the Al-Mg composite's overall strength. The application of powder metallurgy guarantees uniform mixing, accurate microstructure control, and compositional flexibility. It is also scalable and reasonably priced, which makes it the perfect technique for creating Al-Mg/HA composites with the required qualities. This method makes it possible to thoroughly examine the effects of various HA kinds and volume fractions on the performance of the composite, especially concerning mechanical strength, corrosion resistance, and bioactivity in biomedical applications. AMC, Al-xMg/yHAss (x = 5 and 10% volume; y = 10, 15, 20, 30 and 40% volume) was made using powder metallurgy. The same applies to the HA amplifier. The weight criteria listed in Table 1 were used to calculate the weights of the three AMC constituents: magnesium powder, aluminum, and HAss/HA. In this study, MMC reinforcement was provided by HAss and HA. Variations were made to magnesium at 5 and 10 vol%, HAss at 15, 20, 30, and 40 vol%, and HA at 10, 15, 20, 30, and 40 vol%. Weighing the material in the mold with a scale yields a measuring accuracy of ± 0.001 g. These three ingredients are then mixed until they are homogenous, which takes 20 minutes. Subsequently, the uniform blend is inserted into the mold. After that, they are compressed to 650 MPa using a machine press 20 tons. The ideal density and even dispersion of the reinforcing particles are guaranteed by 650 MPa compaction pressure, which improves the mechanical and corrosion resistance qualities. After that, the sample is taken out of the mold. After the sample had solidified, it was sintered by heating it in an oven and maintaining a temperature of 600ºC for two hours. The sintering temperature of 600°C is chosen to guarantee adequate particle bonding without raising the aluminum melting point or changing the bioceramic phases (HA or HAss). The final composite's mechanical qualities and resistance to corrosion are maintained by the two-hour sintering time, which gives the particles enough time to join and avoids excessive grain growth or phase shifts.

The machine is turned off and the sample is left in a hot furnace to cool. Without the use of active cooling equipment, the sample is left to cool naturally in a warm atmosphere. This could be done to lower the sample's temperature gradually without causing thermal shock or fast cooling.

2.2 AMC Manufacturing Procedure

The parameters and process levels of AMC Al-Mg are shown in Table 1.

Table 1. Lists the parameters and levels of the Al-Mg AMC process.

Process parameters	Symbol	Unit	Levels
Aluminum	Al	% vol.	50, 55, 60, 70, 75, 80, 85
Magnesium	Mg	% vol.	5, 10
Snail shell hydroxyapatite	HAss	% vol.	15, 20, 30, 40
Hydroxyapatite	HA	% vol.	10, 15, 20, 30, 40

Al: the broad range (50–85%) denotes various aluminum concentrations that are frequently present in alloys. It also makes it possible to research how it affects composite qualities like strength and resistance to corrosion.

Mg: the two concentrations (5% and 10%) probably correspond to the usual values utilized in alloys made of aluminum and magnesium, which may have a big effect on mechanical characteristics. HA and HAss: a range that frequently influences the mechanical and biological properties of composites is covered by the amounts selected for both HAss and HA (15–40%). Researchers can investigate the materials' bioactivity and reinforcing impact within this range.

2.3 Electrochemical Measurements

A commercially available HBSS powder is dissolved in deionized water to create HBSS. To conform to the physiological conditions of the human body, the pH of the HBSS solution is raised to 7.4. Provide precise instructions for the measurement and preparation processes, especially for the electrochemical testing in HBSS. The working electrode's Open Circuit Potential (OCP) is tracked for 30 minutes to achieve a steady value in the HBSS solution prior to testing. Following the OCP measurement, the potential is scanned in both the anodic and cathodic directions (-250 mV and +250 mV relative to OCP) at a scan rate of 0.5 mV/s to record potentiodynamic polarization curves. The electrochemical studies were conducted using a normal three-electrode cell, where the reference electrode was a Saturated Calomel Electrode (SCE), the working electrode was the sample, and the auxiliary electrode was a platinum plate.

Before conducting electrochemical tests, samples with an open area of 1 cm^2 were submerged in fake blood solution for an hour to stabilize the Open Circuit Potential (OCP). By etching a certain region of the material with a particular amount of electrical potential, potentiodynamic polarization is carried out to ascertain the corrosion current. The values of the potentiostat variables (I_{corr}: corrosion current A/cm^2 and E_{corr}: corrosion potential) were recorded using the slopes identified in the polarization curve of the potentiostat observations. Based on potentiostatic data, the corrosion rate can be calculated using the formula in Eq. 1 [44].

$$CR\ (mpy) = (0.129 \times I_{corr} \times EW)/(\rho \times A) \quad (1)$$

Definition: EW (sample atomic weight/valence electrons = 27.925/3 g), density (ρ = 7.86 g/cm^3), and surface area (A = 1 cm^2) all represent the metal's equivalent weight (g).

For the testing, the voltage range was -3.5 to 3.0 V, the sampling rate was 0.01 V/s, and the operational range was -0.06 to 0.04 A. The corrosion rate is converted from mpy to mmpy using the following formula: 0.0254 mmpy = 1 mpy.

3 Results and Discussion

3.1 Results

Different combinations or quantities of these components in the composites are usually represented by the codes A1-A7 and B1-B7. A1: 80% Al, 5% Mg, 15% HAss; A2: 75% Al, 10% Mg, 15% HAss; A3: 75% Al, 5% Mg, 20% HAss; A4: 70% Al, 10% Mg, 20% HAss; A5: 60% Al, 10% Mg, 30% HAss; and A6: 55% Al, 5% Mg, 40% HAss constitute Group A, which has Al, Mg, and HAss reinforcement. B1: 85% Al, 5% Mg, 10% HA B2: 80% Al, 5% Mg, 15% HA B3: 75% Al, 5% Mg, 20% HA B4: 60% Al, 10% Mg, 30% HA B5: 55% Al, 5% Mg, 40% HA B6: 50% Al, 10% Mg, 40% HA Group B (Al, Mg, and HA) reinforcement.

Table 2 displays the OCP values of AMC Al-Mg/HAss (A1-A7) in the HBSS solution. After the OCP fluctuations subsided and stabilized, measurements were conducted. In comparison to other samples in the HBSS solution, the steady state sample AMC 0.55Al-0.05Mg/0.40HAss (A6), which had a volume fraction of 5% Mg and 40% HAss, had the most negative OCP value (-1.209 V). 120-second exposure period for the first time. Compared to the E_{corr} value (-1240 V), the A6 OCP value (-1209 V) is more

positive. In comparison to the other samples, sample A6 has the lowest I_{corr} value (8.24×10^{-8} A/cm^2). Additionally, sample A6 has the lowest CR value (9.58 x10^{-4} mmpy) according to Table 2 in line with earlier studies [45]. The OCP value increases in this test for A2, A7, A5, A3, A1, and A4 on the AMC.

Table 2. The corrosion properties of AMC with HAss reinforcement.

Kode AMC	OCP (V)	βa (V/dec)	-βc (V/dec)	E_{corr} (V)	I_{corr} (A/cm2)	CR (mmpy)
A1	-1.083	0.161	0.182	-1.21	5.10×10^{-4}	5.93
A2	-1.198	0.162	0.183	-1.27	4.82×10^{-4}	5.60
A3	-1.121	0.101	0.121	-1.27	3.63×10^{-4}	4.22
A4	-0.736	0.049	0.298	-0.36	5.18×10^{-7}	6.02×10^{-3}
A5	-1.121	0.076	0.0842	-1.21	1.95×10^{-4}	2.27
A6	-1.209	0.058	0.058	-1.24	8.24×10^{-8}	9.58×10^{-4}
A7	-1.192	0.191	0.242	-1.27	6.87×10^{-4}	7.98

As a result, even though the corrosion rates of both composites are low, the Al-Mg/HA composite exhibits a corrosion rate that is an order of magnitude lower than that of the Al-Mg/HAss composite. In AMC 0.55Al-0.05Mg/0.40HAss (A6), the cathodic slope (βc) value is less than the anodic slope (βa). Out of all the Al-Mg/HAss AMC samples, this one has the lowest βc value as well. The breakdown of anodic ions into the HBSS solution is indicated by the value βc > βa. In the meantime, two samples from AMC reinforced with HA (B1-B6) are provided in Table 3, 0.50Al-0.10Mg/0.40HA (B6) and 0.80Al-0.05Mg/0.15HA (B2), have βc < βa values. The AMC 0.80Al-0.05Mg/0.15HA (B2) sample has the lowest βc value when compared to the other samples, which are B1, B3, B4, B5, and B6. According to Mehra and Soni, when βc < βa, it means that metal ions at the anode do not dissolve into the test solution [44].

Table 3. The corrosion properties of AMC with HA reinforcement.

Kode AMC	OCP (V)	β_a (V/dec)	$-\beta_c$ (V/dec)	E_{corr} (V)	I_{corr} (A/cm^2)	CR (mmpy)
B1	-1.125	0.274	0.368	-1.26	10.59×10^{-4}	12.31
B2	-0.049	0.027	0.021	-0.87	6.64×10^{-10}	7.72×10^{-6}
B3	-0.491	0.139	0.159	-0.91	1.14×10^{-6}	1.32×10^{-2}
B4	-0.459	0.059	0.090	-1.05	3.62×10^{-6}	4.20×10^{-2}
B5	-0.974	0.147	0.253	-1.18	2.68×10^{-6}	3.11
B6	-0.434	0.282	0.116	-0.64	3.17×10^{-6}	3.68×10^{-2}

Fig. 1 displays the polarization curve of the AMC Al-Mg/HAss composite in HBSS solution at various material volume fractions. It contributed to the analysis of corrosion behavior. I_{corr}, E_{corr}, βa, and βc are the corrosion parameters that can be determined by extrapolating the polarization curve [46]. HAss and HA are the two forms of reinforcing particles employed. Only the active behavior in the potential area without a passive zone is depicted in this diagram. The corrosion current density (I_{corr}) for AMC 0.50Al-0.10Mg/0.40HAss and 0.55Al-0.05Mg/0.40HA has the greatest value of 6.87×10^{-4} and the lowest value of 8.25×10^{-8} A/cm^2. AMC 0.50Al-0.10Mg/0.40HAss has the most active E_{corr} value, -1.2729 V, whereas AMC 0.70Al-0.10Mg/0.20HAss has the highest E_{corr} value, -0.36 V. AMC Al-Mg/HAss exhibits non-symmetric anode and cathode curves, with the cathode curve exhibiting strong linearity. The passivation characteristics and polarization curves of Al-Mg/HAss AMC composites are often the same (Fig. 1).

By extrapolating the Tafel diagram, the E_{corr} and I_{corr} of all Al-Mg/HA AMC materials were found (Table 3). AMC Al-Mg/HAss E_{corr} and I_{corr} clearly show that variations in the volume ratio of AMC Al-Mg/HA and the volume fraction of reinforcement do not follow a consistent pattern. On the other hand, as the HAss volume climbed and the Mg volume portion was 5%, the corrosion current density dropped. HA reinforcement with a 15% volume fraction had the lowest I_{corr} value at the same Mg value. By projecting the cathodic curve to the corrosion potential, this curve is utilized to determine the corrosion current density [47]. In Tafel extrapolation, the AMC Al-Mg/HAss potential value is -3.5 V to 3.0 V more negative than the corrosion potential. Sample A7 had the highest corrosion current density. Following the addition of 20 vol% HAss and 10 vol% Mg, the Al-Mg/HAss AMC's corrosion current density dropped to 8.25×10^{-8} A/cm^2.

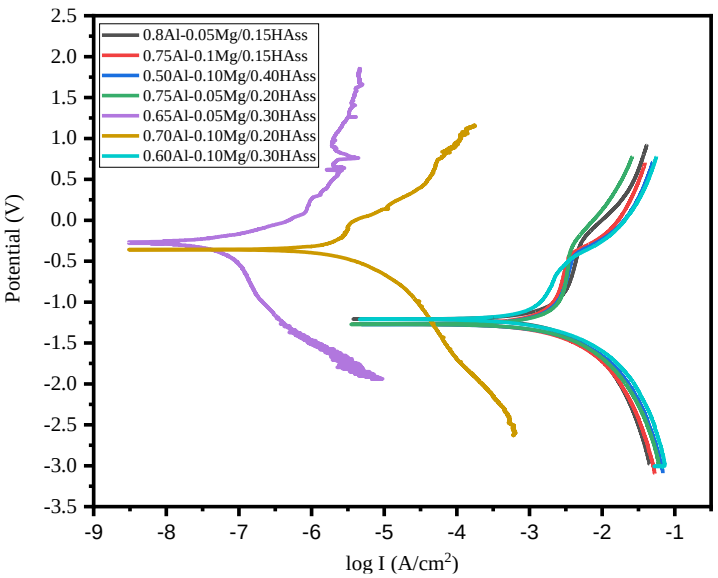

Fig. 1. Tafel polarisation curves of Al-Mg/HAss composite in HBSS solutions.

By altering the alloy's electrochemical behavior and acting as a protective layer or reinforcing phase, HAss might lessen the alloy's vulnerability to corrosion. By creating a more stable surface layer or lowering the local electrolyte concentration surrounding the alloy, HAss may be able to lessen the harmful effects of chloride ions and prevent corrosion from starting and spreading. Furthermore, the alloy's microstructure may be altered by the hydroxyapatite particles, decreasing its vulnerability to attack by chloride. Increased hardness or surface integrity, two mechanical qualities that could contribute to greater corrosion resistance, could be the outcome of reinforcing the Al-Mg matrix with HAss.

Pitting corrosion can easily occur since the passive area is nearly unnoticeable, as seen by the Tafel diagram (Fig. 1). Among the AMC samples, sample A4 exhibits the greatest E_{corr} value (-0.36 V). The sample E_{corr} values, A1 (-1.21 V), A5 (-1.21 V), A6 (-1.24 V), A2 (-1.27 V), A3 (-1.27 V), and A7 (-1.27 V), range from more positive to more negative. Sample A7 had the highest I_{corr} at -6.87×10^{-4} A/cm^2. The samples A1 (-5.11×10^{-4} A/cm^2), A2 (-4.82×10^{-4} A/cm^2), A3 (-3.63×10^{-4} A/cm^2), A5 (-1.95×10^{-4} A/cm^2), A4 (-5.18×10^{-7} A/cm^2), and A6 (-8.25×10^{-8} A/cm^2) are then examined. According to these findings, the AMC Al/Mg-HAss sample, which has a CR value of 9.6×10^{-4} mmpy, exhibits the best corrosion resistance in AMC with Al 55 vol%, Mg 5%, and HAss 40%. Nearly identical AMC A7, A5, A4, A3, A2, and A1 E_{corr} range from -1.21 V to -1.27 V. The potential that corresponds to this transitory current is known as the critical potential E_{pit} [48], and this sharp increase in current density suggests a steady point input. Compared to MMC A6, which has an E_{corr} of -1.24 V, AMC A4 has a higher positive E_{corr} of -0.36 V. In contrast to AMC A4 (I_{corr} = 5.18×10^{-7} A/cm^2), AMC A6 exhibits a lower I_{corr} of 8.25×10^{-8} A/cm^2, indicating the addition of magnesium to the 5%. On an Al matrix, 40% HAss at 55% volume and 40% magnesium powder by volume exhibit higher corrosion resistance.

The addition of HA and Mg to AMC significantly alters the corrosion potential and corrosion current density, as shown by the

potentiodynamic polarization curve in Fig. 2 and the Tafel configuration data in Table 2. There are three zones on the Tafel curve: the active, passive, and transpassive regions. The corrosion current density rose from 6.60×10^{-10} to 1.06×10^{-3} A/cm^2 with the addition of HA and Mg volume fractions to Al-Mg/HA AMC. With a value of 1.06×10^{-3} A/cm^2, the 0.85Al-0.05Mg/0.10HA (B1) sample had the highest corrosion current density. The AMC Al-Mg/HA corrosion current density dropped to 6.60×10^{-10} A/cm^2 upon the addition of 5 vol% Mg and 15 vol% HA fraction. Anodic breakdown takes place in regions of activity. When E_{corr} values are compared, E_{corr} B2 is more negative than E_{corr} B6, but slightly more positive than E_{corr} B3 and B4. The I_{corr} in this area grows exponentially as potential increases. The AMC B2 sample's I_{corr} value indicates that it transfers less free and intermediate AMC cations than other samples. In quiet areas where productive species are anticipated and oxide production takes place. It is evident that the maximum I_{corr} and the passive constant current density (Ip) in this region are equal. With a constant or decreasing current density, B2's potential area is nearly identical to that of the other samples. The current density is observed to increase fast in the transpassive zone, suggesting that anodic melting is taking place once more.

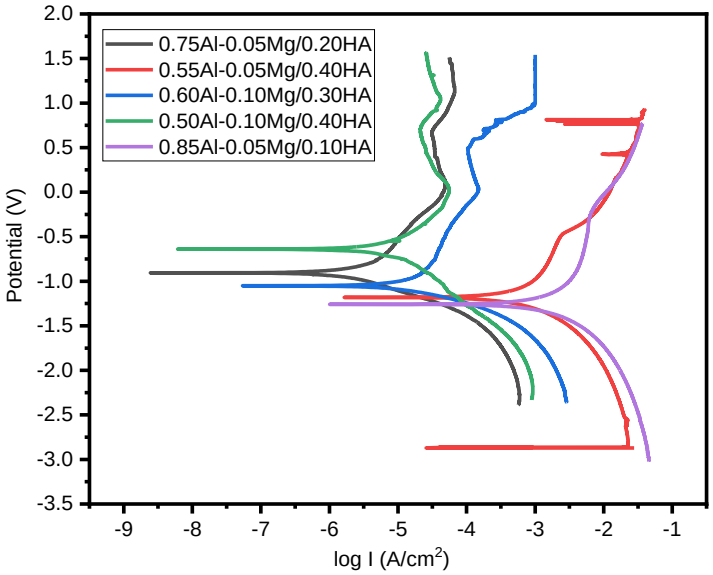

Fig. 2. Tafel polarisation curves of Al-Mg/HA composite in HBSS solutions.

When the reinforcement is 40 vol% (composite A), the corrosion current density of the HAss reinforced with Al-Mg AMC can be very low or even very high, as shown by the distribution of the I_{corr} of AMC in Fig. 3. The I_{corr} will be extremely low (minimum) if you use 5 vol% Mg and 55 vol% Al. In actuality, it depends on the Mg composition. But when 10 vol% Mg is used, the I_{corr} increases significantly to 50 vol% (highest). The I_{corr} value is large because Al-Mg AMC with 20 vol% HAcs strengthening employs 5 vol% Mg and 75 vol% Al. Conversely, the I_{corr} value is significantly lower when 10 vol% Mg and 70 vol% Al are used. When a 15% v/v HAss boost is applied, the I_{corr} values produced with 10% v/v and 5% Mg are nearly identical. In contrast, the highest I_{corr} value was achieved at 10 vol% HA reinforcement in Al-Mg MMC (composite B) is provided in Fig. 4, while the lowest I_{corr} value was seen at 15 vol% HA reinforcement.

AMC 0.55Al-0.05Mg/0.40HAss has the lowest corrosion rate among AMC Al-Mg reinforced with HAss, as can also be seen from the CR value (sample A). The MMC corrosion rate decreases as the volume fraction of HAss reinforcement increases when a 5% Mg volume fraction is used in Al-MMC; the lowest corrosion rate is attained at 40% HAss reinforcement. The corrosion rate of AMC Al-Mg/HAss decreases with increasing HAss volume fraction with 5% Mg, and 40% of HAss volume is optimal for corrosion resistance. The corrosion rate does not, however, follow the same pattern when 10% Mg is used instead of 5% Mg reinforced with HA. Of all the B samples, sample B's Al-Mg AMC with HA reinforcement (AMC 0.80Al-0.05Mg/0.15HA) has the lowest corrosion rate.

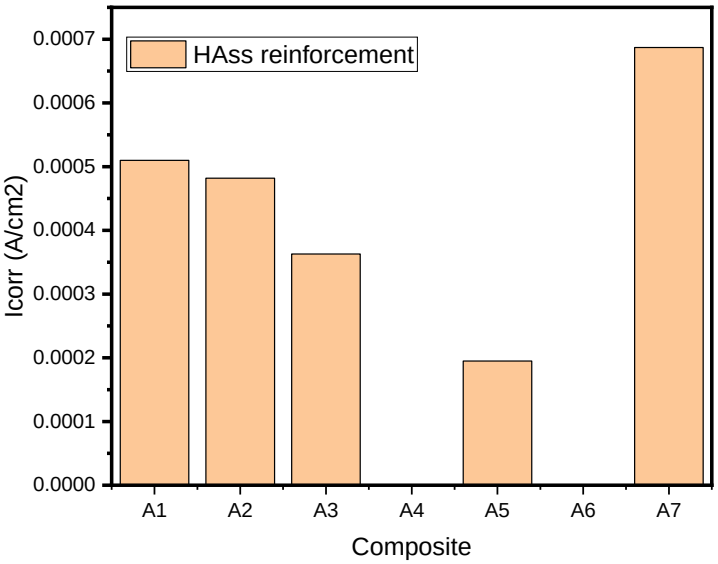

Fig. 3. Variation of Al-Mg/Hass corrosion current density in HBSS solution.

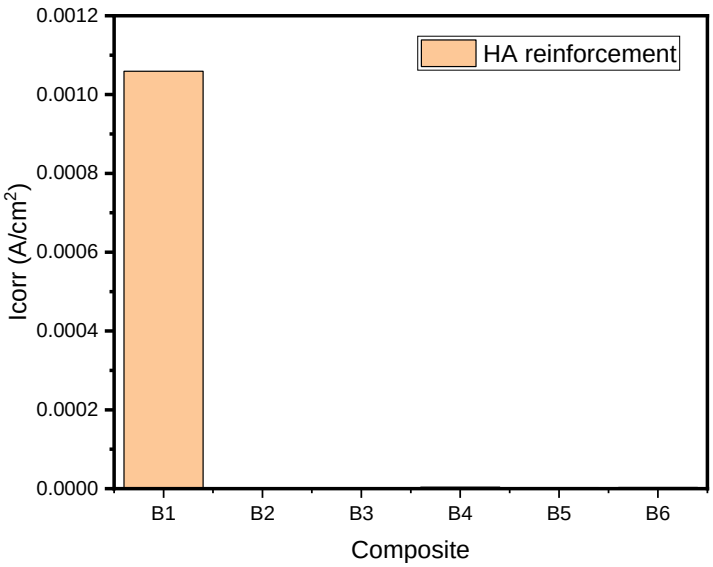

Fig. 4. Variation of Al-Mg/HA corrosion current density in HBSS solution.

The study can evaluate the impacts of hydroxyapatite reinforcements on mechanical properties and corrosion resistance in a controlled way thanks to the combination of particular volume fractions (40% HAss and 15% HA) and powder metallurgy. PM is the perfect technique for creating high-performance aluminum-magnesium matrix composites because it provides benefits such as consistent distribution, accurate control over composite composition, and cost-effectiveness.

3.2 Discussion

Adding reinforcing particles can improve AMC's corrosion resistance, as the literature analysis notes. The corrosion rate of Al-Mg AMC with and without HAss reinforcing is investigated and analyzed in this work. According to the current study, adding HAss particles improved AMC's ability to withstand corrosion in high Cl environments. Cl^-, an active anion with significant adsorption and erosion capabilities, is primarily responsible for pitting corrosion [49]. Wei et al. claim that the oxide layer on the surface of aluminum acts as a barrier to prevent matrix corrosion

[50]. Pitting is a kind of erosion hole that starts in a small spot on the sample's surface and moves deep into the metal, gradually expanding in depth and diameter as it creates corrosion holes. Pitting corrosion, the most prevalent type of corrosion in aluminum alloys, eventually gives way to more severe corrosion, like stress corrosion cracking [51]. The most obvious defects are caused by pitting corrosion. Recent research on aluminum alloys has shown that the substrate and the two-phase particles deteriorate at different rates, producing heterogeneous oxide layer thicknesses [52].

The present work shows that Al-Mg composites' corrosion resistance is enhanced by both synthetic and natural hydroxyapatite, with HA exhibiting marginally superior performance. The findings are consistent with earlier research on bioceramic-reinforced Al-Mg composites, where HA significantly improved corrosion resistance. Nonetheless, the corrosion rates of Al-Mg composites are still higher than those of coatings such as ZrO_2/TiO_2 on Ti-6Al-4V alloys [53]. This is to be expected given the intrinsic qualities of titanium alloys and the extra advantages of homogeneous, high-quality coatings for substrate protection. Optimizing reinforcement techniques for aluminum-based composites in demanding situations is made easier by being aware of these parallels and differences.

A greater OCP value is indicative of an anodic response. The rate of corrosion is higher in the anode area because the OCP value is higher than the E_{corr} value. Surface corrosion is not uniform in the cathode area, as indicated by the OCP value being lower than E_{corr}. The OCP value is determined by the chemical composition of the AMC. The variations in OCP values seen in AMC are typical of material systems that experience passive layer formation and recurrent degradation in a corrosive environment [54]. AMC 0.80Al-0.05Mg/0.15HA (B2) has the strongest corrosion resistance in the HBSS solution because it has the highest OCP value and moves positively. Next were samples AMC B6, B4, B3, B5, and B1. These findings imply that, in chloride-rich environments, the concentration of Cl ions affects Al-Mg/HA AMCs' corrosion resistance and thermodynamic stability without the need for potential. In contrast to samples without chloride, the OCP value in samples alloyed with chloride decreased rapidly as a result of repassivation. The OCP value is relatively constant over a narrow potential range, but thermodynamically unstable until the latter hours of continuous oscillation [55]. The OCP series is in good agreement with data on aluminum alloys from the same solutions [56]. The OCP of every sample was rather constant because of the passive film formation that occurred throughout testing. The little oscillations observed in each OCP curve are caused by the point repair and repassivation processes. OCP, a measure of an alloy's susceptibility to corrosion, is influenced by the solute content in the matrix [57]. However, due to microgalvanic processes, holes are usually formed by heterogeneous microstructures [58].

The B6 E_{corr} sample (-0.64 V) is more positive than the other samples (-0.87 V B2, -0.91 V (B3), -1.05 V (B4), -1.18 V (B5), and -1.26 V (B1) (Table 2). Fig. 2's potentiodynamic polarization curve illustrates the comparable polarization tendency concerning positional changes. The first four curves, B2, B4, B6, and B3, show an increasing degree of surface passivity by showing a decrease in current density and an increase in potential. Although there is very little potential difference, the passive zone forms in the polarization curve of the AMC B5 sample but has not yet developed in the B1 curve. The sample with the lowest I_{corr}, measured at 6.60×10^{-10} A/cm^2, is B2; subsequent samples had I_{corr} of 3.62×10^{-6} A/cm^2, 3.17×10^{-6} A/cm^2), B3 (1.14×10^{-6} A/cm^2), B5 (2.68×10^{-4} A/cm^2), and B1 (1.06×10^{-3} A/cm^2). The elemental composition of AMC that exhibits the best corrosion resistance is composed of 80% AI (0.80 Al-0.05 Mg/0.15 HA), 15% HA, and 5% magnesium by volume. Although pick-up corrosion, which Zaid et al. also observed, was not observed, the notable increase in sample current density indicates that $E_{pit} = E_{corr}$ [59]. The decrease in corrosion resistance of aluminum alloys after annealing may be due to the microstructural characteristics of the alloy during annealing, which creates a microstructure with fewer defects. This may be because the alloy structure's point defects, dislocation density, and grain size all decrease with annealing, resulting in fewer defects in the protective layer [60].

The Al-Mg I_{corr} AMC values with 20 and 30% HA strengthening differ just slightly. Compared to the same HA reinforcement with a 10% Mg and 50% Al matrix, the I_{corr} value is lower for 40 vol% reinforcement with a 5% Mg and 55% Al matrix. This suggests that AMC in compound A is less prone to corrosion in the HBSS 0.70Al-0.10Mg/0.20HAss solution than other compounds. The combination of 0.80Al-0.05Mg/0.15HA for the B AMC Al-Mg composite reinforced with HA showed the highest corrosion resistance when compared to other treatments. Current density and corrosion rate are strongly related because concentrated current in a small area produces a high corrosion rate. The potential difference between the two phases and the Al matrix accelerates local corrosion at the interface between the second phase particles and the Al-Mg alloy matrix [61]. Although increasing grain size results in smaller grain borders, increasing the proportion of low-angle grain boundaries implies reduced misorientation of the grain structure, resulting in a more uniform structure with fewer flaws and higher corrosion performance [62]. Aluminum composites are said to be susceptible to galvanic corrosion due to the possibility of fracture between the reinforcement and the aluminum matrix [63].

Aluminum alloys can readily undergo passivation to produce speck formation when active anions such as Cl are present. Rusty film covering the surface. However, there are certain disadvantages to naturally oxidized films, such as their softness, low resistance to corrosion, thinness, and breakability. When active anions, like Cl^-, are present in the environment, they speed up the breakdown of the natural oxide layer and cause corrosion pits. Once produced, the Al metal in the corrosion hole dissolves more quickly due to the influence of the big cathode and small anode. The rapid decomposition of aluminum metal in the anode hole increases the concentration of Al^{3+}, and as Al^{3+} is hydrolyzed quickly, the environment of the well becomes more acidic. As the quantity of positive ions in the anode process increases, external Cl^- is forced to diffuse into the hole, raising the concentration of Cl^- in the hole. Additionally, certain corrosion products are trapped in holes that are both internal and external and have wildly different conditions [64]. AMC corrosion resistance is increased by the passive layer that forms on the sample surface as a result of the oxygen atom reduction reaction. With additional exposure to chlorine corrosion, the resulting passivation becomes more unstable and finally degrades to the point of forming isolated patches [65].

Active deposition is the outcome of biofilm calcification, in which the labile part of a biofilm continuously degrades, regenerates, and releases calcium together with the matrix. If the amount of calcium is more than what can be bound and the biofilm increases the pH of the surrounding environment by reducing oxygen, calcium precipitates, leading to passive deposition [66]. Ralston et al. [67] present the correlation between average grain size and corrosion rate for several alloys. According to this paper, the impact of grain size on the rate of metal corrosion can be estimated using the Eq. 2.

$$I_{corr} = \alpha + \beta(G.S.)^{-0.5} \quad (2)$$

The constant in this equation represents the corrosive medium; it is a material-dependent constant that varies according to the kind and concentration of pollutants. The corrosion rate is directly proportional to the inverse of the square root of the grain size, according to this model. Corrosion is therefore driven by electrical

communication between the cathodic and anodic portions of the grains when high-energy grain borders are present. The movement or penetration of oxide ions is the characteristic corrosion mechanism of this occurrence, initially weakening and then eliminating the passive oxide layer [68]. Because of viscosity and reinforcement agglomeration, porosity is produced as the reinforcement fraction increases along with the rate of AMC corrosion.

4 Conclusion

After the contents are removed, snail shell particles, or HAss, are wasted. They contain a lot of calcium oxide and can be utilized as a composite reinforcing material to create ecological materials. The process of powder metallurgy is used to create Al-Mg AMC. This study demonstrates how adding HAcs to Al-Mg AMC changed its corrosion behavior. The study's findings were contrasted with those of Al-Mg AMC strengthened with HA. For every Al-Mg/HAss AMC model, HAss improves the corrosion resistance of Al-Mg AMC in HBSS solution at a variable rate of corrosion. Al-Mg/HAss AMCs are more resistant to corrosion because of the thin barrier layer that HAss creates, which strengthens the oxide layer. At a 40% HAss reinforcement and a 5% Mg volume fraction, the ideal Al-Mg AMC structure is discovered. The lowest corrosion rate is 9.58×10^{-4} mmpy for AMC Al-Mg/HAss, which is present in AMC 0.55Al-0.05Mg/0.40 HAss. In the meantime, MMC Al-Mg/HA had the lowest corrosion rate, 7.72×10^{-6} mmpy for AMC 0.80Al-0.05Mg/0.15HA. The corrosion resistance of AMC in HBSS solution is increased when HA containing $CaCO_3$ is added to Al-Mg AMC. To further understand how to optimize these composites for practical uses, more research might also examine the precise mechanisms by which HAss increases corrosion resistance in Al-Mg matrices. Overall, even though the results are encouraging, more thorough research and testing would be beneficial for the real-world use of HAss in biomaterials.

References

[1] F. C. Campbell, "Introduction and Uses of Lightweight Materials," *Light. Mater. Underst. Basics*, p. 4, 2012.

[2] A. Contreras, C. A. León, R. A. L. Drew, and E. Bedolla, "Wettability and spreading kinetics of Al and Mg on TiC," *Scr. Mater.*, vol. 48, no. 12, pp. 1625–1630, 2003, doi: 10.1016/S1359-6462(03)00137-4.

[3] W. Wulandari, G. A. Brooks, M. a Rhamdhani, and B. J. Monaghan, "Magnesium : Current and Alternative Production Routes," *Chemeca 2010 Eng. Edge; 26-29 Sept. 2010, Hilt. Adelaide, South Aust.*, p. 347, 2010.

[4] N. Kumar, A. Gautam, R. S. Singh, and M. K. Manoj, "Study of B4C/Al–Mg–Si Composites as Highly Hard and Corrosion-Resistant Materials for Industrial Applications," *Trans. Indian Inst. Met.*, vol. 72, no. 9, pp. 2495–2501, 2019, doi: 10.1007/s12666-019-01717-w.

[5] K. M. Youssef, R. O. Scattergood, K. L. Murty, and C. C. Koch, "Nanocrystalline Al-Mg alloy with ultrahigh strength and good ductility," *Scr. Mater.*, vol. 54, no. 2, pp. 251–256, 2006, doi: 10.1016/j.scriptamat.2005.09.028.

[6] R. A. Sielski, "Research needs in aluminum structure," *10th Int. Symp. Pract. Des. Ships other Float. Struct. PRADS 2007*, vol. 2, pp. 960–967, 2007.

[7] E. L. Huskins, B. Cao, and K. T. Ramesh, "Strengthening mechanisms in an Al-Mg alloy," *Mater. Sci. Eng. A*, vol. 527, no. 6, pp. 1292–1298, 2010, doi: 10.1016/j.msea.2009.11.056.

[8] L. jing Bai, G. Kou, K. Zhao, G. Tao Chen, and F. Xue Yan, "Effect of in-situ micro-arc oxidation coating on the galvanic corrosion of AZ31Mg coupled to aluminum alloys," *J. Alloys Compd.*, vol. 775, pp. 1077–1085, 2019, doi: 10.1016/j.jallcom.2018.10.154.

[9] S. E. Vannan and S. P. Vizhian, "Microstructure and Mechanical Properties of as Cast Aluminium Alloy 7075/Basalt Dispersed Metal Matrix Composites," *J. Miner. Mater. Charact. Eng.*, vol. 02, no. 03, pp. 182–193, 2014, doi: 10.4236/jmmce.2014.23023.

[10] Z. Zuliantoni, W. Suprapto, P. H. Setyarini, and F. Gapsari, "Extraction and characterization of snail shell waste hydroxyapatite," *Results Eng.*, vol. 14, no. November 2021, p. 100390, 2022, doi: 10.1016/j.rineng.2022.100390.

[11] K. D. Ahalya and B. Kandasubramanian, "Revolutionizing biomedical engineering: Extrusion-based hydroxyapatite printing for scaffold construction: A review," *Hybrid Adv.*, vol. 6, no. March, p. 100227, 2024, doi: 10.1016/j.hybadv.2024.100227.

[12] G. C. Onuegbu and I. O. Igwe, "The Effects of Filler Contents and Particle Sizes on the Mechanical and End-Use Properties of Snail Shell Powder Filled Polypropylene," *Mater. Sci. Appl.*, vol. 02, no. 07, pp. 810–816, 2011, doi: 10.4236/msa.2011.27110.

[13] S. Kaewdaeng and R. Nirunsin, "Synthesis of calcium oxide from river snail shell as a catalyst in production of biodiesel," *Appl. Environ. Res.*, vol. 41, no. 1, pp. 31–37, 2019, doi: 10.35762/AER.2019.41.1.4.

[14] K. M. Balabadra, S. Panneer Selvam, R. Ramadoss, and S. Sundar, "Hydroxyapatite synthesis and characterization from marine sources: A comparative study," *J. Oral Biol. Craniofacial Res.*, vol. 14, no. 6, pp. 706–711, 2024, doi: 10.1016/j.jobcr.2024.09.009.

[15] J. Anita Lett *et al.*, "Bone tissue engineering potentials of 3D printed magnesium-hydroxyapatite in polylactic acid composite scaffolds," *Artif. Organs*, vol. 45, no. 12, pp. 1501–1512, 2021, doi: 10.1111/aor.14045.

[16] L. Xiang, Y. Xiang, Y. Wen, and F. Wei, "Formation of CaCO3 nanoparticles in the presence of terpineol," *Mater. Lett.*, vol. 58, no. 6, pp. 959–965, 2004, doi: 10.1016/j.matlet.2003.07.034.

[17] W. Zhang, S. Yamashita, and H. Kita, "Progress in tribological research of SiC ceramics in unlubricated sliding-A review," *Mater. Des.*, vol. 190, p. 108528, 2020, doi: 10.1016/j.matdes.2020.108528.

[18] N. F. Syamimi, M. R. Islam, M. G. Sumdani, and N. M. Rashidi, "Mechanical and thermal properties of snail shell particles-reinforced bisphenol-A bio-composites," *Polym. Bull.*, vol. 77, no. 5, pp. 2573–2589, 2020, doi: 10.1007/s00289-019-02878-w.

[19] M. Olivia, A. A. Mifshella, and L. Darmayanti, "Mechanical properties of seashell concrete," *Procedia Eng.*, vol. 125, pp. 760–764, 2015, doi: 10.1016/j.proeng.2015.11.127.

[20] N. A. S. Mohd Pu'ad, P. Koshy, H. Z. Abdullah, M. I. Idris, and T. C. Lee, "Syntheses of hydroxyapatite from natural sources," *Heliyon*, vol. 5, no. 5, p. e01588, 2019, doi: 10.1016/j.heliyon.2019.e01588.

[21] S. Santhosh and S. Balasivanandha Prabu, "Thermal stability of nano hydroxyapatite synthesized from sea shells through wet chemical synthesis," *Mater. Lett.*, vol. 97, pp. 121–124, 2013, doi: 10.1016/j.matlet.2013.01.081.

[22] P. A. F. Sossa, B. S. Giraldo, B. C. G. Garcia, E. R. Parra, and P. J. A. Arango, "Comparative study between natural and synthetic hydroxyapatite: Structural, morphological and bioactivity properties," *Rev. Mater.*, vol. 23, no. 4, 2018, doi: 10.1590/s1517-707620180004.0551.

[23] C. Prakash and S. Singh, "On the characterization of functionally graded biomaterial primed through a novel plaster mold casting process," *Mater. Sci. Eng. C*, vol. 110, no. January, p. 110654, 2020, doi: 10.1016/j.msec.2020.110654.

[24] S. kumar Balu, S. Andra, J. Jeevanandam, M. V. S, and S. V, "Emerging marine derived nanohydroxyapatite and their

composites for implant and biomedical applications," *J. Mech. Behav. Biomed. Mater.*, vol. 119, no. April, p. 104523, 2021, doi: 10.1016/j.jmbbm.2021.104523.
[25] J. Singh, C. S. Jawalkar, and R. M. Belokar, "Analysis of Mechanical Properties of AMC Fabricated by Vacuum Stir Casting Process," *Silicon*, vol. 12, no. 10, pp. 2433–2443, 2020, doi: 10.1007/s12633-019-00338-8.
[26] X. Ji, C. Zhang, and S. Li, "In Situ Synthesis of Core-Shell-Structured SiCp Reinforcements in Aluminium Matrix Composites by Powder Metallurgy," *Metals (Basel).*, 2021.
[27] M. Ali, M. A. Hussein, and N. Al-Aqeeli, "Magnesium-based composites and alloys for medical applications: A review of mechanical and corrosion properties," *J. Alloys Compd.*, vol. 792, pp. 1162–1190, 2019, doi: 10.1016/j.jallcom.2019.04.080.
[28] Y. Yang *et al.*, "Mg bone implant: Features, developments and perspectives," *Mater. Des.*, vol. 185, p. 108259, 2020, doi: 10.1016/j.matdes.2019.108259.
[29] N. Kumar and S. Soren, "Selection of reinforcement for Al/Mg alloy metal matrix composites," *Mater. Today Proc.*, vol. 21, pp. 1605–1609, 2020, doi: 10.1016/j.matpr.2019.11.238.
[30] D. Saber, R. Abdel-Karim, A. A. Kandel, and K. A. El-Aziz, "Corrosive Wear of Alumina Particles Reinforced Al–Si Alloy Composites," *Phys. Met. Metallogr.*, vol. 121, no. 2, pp. 188–194, 2020, doi: 10.1134/S0031918X19120147.
[31] A. Tahmasebifar, S. M. Kayhan, Z. Evis, A. Tezcaner, H. Çinici, and M. Koç, "Mechanical, electrochemical and biocompatibility evaluation of AZ91D magnesium alloy as a biomaterial," *J. Alloys Compd.*, vol. 687, pp. 906–919, 2016, doi: 10.1016/j.jallcom.2016.05.256.
[32] S. Johnston, Z. Shi, and A. Atrens, "The influence of pH on the corrosion rate of high-purity Mg, AZ91 and ZE41 in bicarbonate buffered Hanks' solution," *Corros. Sci.*, vol. 101, pp. 182–192, 2015, doi: 10.1016/j.corsci.2015.09.018.
[33] C. J. Lin, R. G. Du, and T. Nguyen, "In-situ imaging of chloride ions at the metal/solution interface by scanning combination microelectrodes," *Corrosion*, vol. 56, no. 1, pp. 41–47, 2000, doi: 10.5006/1.3280521.
[34] F. Sun *et al.*, "Effect of Sc and Zr additions on microstructures and corrosion behavior of Al-Cu-Mg-Sc-Zr alloys," *J. Mater. Sci. Technol.*, vol. 33, no. 9, pp. 1015–1022, 2017, doi: 10.1016/j.jmst.2016.12.003.
[35] G. S. Frankel and N. Sridhar, "Understanding localized corrosion," *Mater. Today*, vol. 11, no. 10, pp. 38–44, 2008, doi: 10.1016/S1369-7021(08)70206-2.
[36] Jaiswal, R. M. Kumar, P. Gupta, M. Kumaraswamy, and P. Roy, "Behavior of Biomedical Materials Mechanical , corrosion and biocompatibility behaviour of Mg-3Zn-HA biodegradable composites for orthopaedic fi xture accessories," *J. Mech. Behav. Biomed. Mater.*, vol. 78, no. October 2017, pp. 442–454, 2018, doi: 10.1016/j.jmbbm.2017.11.030.
[37] R. Radha and D. Sreekanth, "Mechanical and corrosion behaviour of hydroxyapatite reinforced Mg-Sn alloy composite by squeeze casting for biomedical applications," *J. Magnes. Alloy.*, vol. 8, no. 2, pp. 452–460, 2020, doi: 10.1016/j.jma.2019.05.010.
[38] A. Aiello and K. Sieradzki, "Corrosion of Binary Mg-Al Alloys," *J. Electrochem. Soc.*, vol. 165, no. 14, pp. C950–C961, 2018, doi: 10.1149/2.0771814jes.
[39] K. H. Choi *et al.*, "Effect of combined extrusion and rolling parameters on mechanical and corrosion properties of new high strength Al-Mg alloy," *Metals (Basel).*, vol. 11, no. 3, pp. 1–10, 2021, doi: 10.3390/met11030445.
[40] N. S. Kim, S. H. Ha, Y. O. Yoon, G. Y. Yeom, H. K. Lim, and S. K. Kim, "Effect of Mg contents on fluidity of Al-xMg alloys," *Miner. Met. Mater. Ser.*, no. 210869, pp. 453–456, 2016, doi: 10.1007/978-3-319-65136-1_78.
[41] D. M. Jiang, S. B. Kang, and H. W. Kim, "Microstructure and mechanical properties of Al-Mg alloy sheets for autobody application," *Mater. Sci. Technol.*, vol. 15, no. 12, pp. 1401–1407, 1999, doi: 10.1179/026708399101505536.
[42] A. Pramono, F. Sulaiman, and A. Milandia, "Fabrication of metal matrix composites based on hydroxyapatite by self-high propagating temperatures synthesis (SHS)," no. August, 2020, doi: 10.20944/preprints202008.0596.v1.
[43] X. Gu, W. Zhou, Y. Zheng, L. Dong, Y. Xi, and D. Chai, "Microstructure , mechanical property , bio-corrosion and cytotoxicity evaluations of Mg / HA composites," *Mater. Sci. Eng. C*, vol. 30, no. 6, pp. 827–832, 2010, doi: 10.1016/j.msec.2010.03.016.
[44] R. Mehra and A. Soni, "Cast iron deterioration with time in various aqueous salt solutions," *Bull. Mater. Sci.*, vol. 25, no. 1, pp. 53–58, 2002, doi: 10.1007/BF02704595.
[45] A. Hossain, F. Gulshan, and A. S. W. Kurny, "Electrochemical investigation of corrosion behavior heat treated al-6si-0.5Mg- x Cu (x = 0, 0.5, 1, 2, and 4 wt%) alloys," *Int. J. Corros.*, vol. 2014, pp. 1–7, 2014, doi: 10.1155/2014/356752.
[46] Y. Feng, X. Li, R. Wang, C. Peng, and L. Liu, "Influence of cerium on microstructures and electrochemical properties of Al-Mg-Sn-Hg anode materials for seawater battery," *J. Rare Earths*, vol. 33, no. 9, pp. 1010–1016, 2015, doi: 10.1016/S1002-0721(14)60519-6.
[47] N. Wang, R. Wang, C. Peng, Y. Feng, and B. Chen, "Effect of hot rolling and subsequent annealing on electrochemical discharge behavior of AP65 magnesium alloy as anode for seawater activated battery," *Corros. Sci.*, vol. 64, pp. 17–27, 2012, doi: 10.1016/j.corsci.2012.06.024.
[48] D. A. Jones, "Principles and prevention of corrosion, Prentice-Hall International, NJ, USA," 1996.
[49] J. J. S. Rodríguez, F. J. S. Hernández, and J. E. G. González, "The effect of environmental and meteorological variables on atmospheric corrosion of carbon steel, copper, zinc and aluminium in a limited geographic zone with different types of environment," *Corros. Sci.*, vol. 45, no. 4, pp. 799–815, 2003, doi: 10.1016/S0010-938X(02)00081-1.
[50] X. Wei, C. Dong, Z. Chen, K. Xiao, and X. Li, "A DFT study of the adsorption of O2 and H2O on Al(111) surfaces," *RSC Adv.*, vol. 6, no. 61, pp. 56303–56312, 2016, doi: 10.1039/c6ra08958e.
[51] P. Xia, Z. Liu, S. Bai, L. Lu, and L. Gao, "Enhanced fatigue crack propagation resistance in a superhigh strength Al–Zn–Mg–Cu alloy by modifying RRA treatment," *Mater. Charact.*, vol. 118, pp. 438–445, 2016, doi: 10.1016/j.matchar.2016.06.023.
[52] K. D. Ralston, N. Birbilis, M. Weyland, and C. R. Hutchinson, "The effect of precipitate size on the yield strength-pitting corrosion correlation in Al-Cu-Mg alloys," *Acta Mater.*, vol. 58, no. 18, pp. 5941–5948, 2010, doi: 10.1016/j.actamat.2010.07.010.
[53] M. Chellappa and U. Vijayalakshmi, "Improved corrosion resistant and mechanical behavior of distinct composite coatings (silica/titania/zirconia) on Ti–6Al–4V deposited by EPD," *J. Asian Ceram. Soc.*, vol. 5, no. 3, pp. 326–333, 2017, doi: 10.1016/j.jascer.2017.06.005.
[54] K. Kanayo Alaneme and P. Apata Olubambi, "Corrosion and wear behaviour of rice husk ash - Alumina reinforced Al-Mg-Si alloy matrix hybrid composites," *J. Mater. Res. Technol.*, vol. 2, no. 2, pp. 188–194, 2013, doi: 10.1016/j.jmrt.2013.02.005.
[55] R. T. Loto and P. Babalola, "Corrosion polarization behavior and microstructural analysis of AA1070 aluminium silicon carbide matrix composites in acid chloride concentrations,"

Cogent Eng., vol. 4, no. 1, 2017, doi: 10.1080/23311916.2017.1422229.
[56] O. Seri, "The effect of NaCl concentration on the corrosion behavior of aluminum containing iron," *Corros. Sci.*, vol. 36, no. 10, pp. 1789–1803, 1994, doi: 10.1016/0010-938X(94)90132-5.
[57] L. Mei, X. P. Chen, C. Wang, J. Xie, and Q. Liu, "Good combination of strength and corrosion resistance in an Al-Cu-Mg alloy processed by a short-cycled thermomechanical treatment," *Mater. Charact.*, vol. 181, no. July, p. 111469, 2021, doi: 10.1016/j.matchar.2021.111469.
[58] N. Wegner and F. Walther, "Assessment of galvanostatic anodic polarization to accelerate the corrosion of the bioresorbable magnesium alloy we43," *Appl. Sci.*, vol. 11, no. 5, pp. 1–15, 2021, doi: 10.3390/app11052128.
[59] B. Zaid, D. Saidi, A. Benzaid, and S. Hadji, "Effects of pH and chloride concentration on pitting corrosion of AA6061 aluminum alloy," *Corros. Sci.*, vol. 50, no. 7, pp. 1841–1847, 2008, doi: 10.1016/j.corsci.2008.03.006.
[60] B. Bobić, S. Mitrović, M. Babić, and I. Bobić, "Corrosion of Metal-Matrix composites with aluminium alloy substrate," *Tribol. Ind.*, vol. 32, no. 1, pp. 3–11, 2010.
[61] S. Annamalai, S. Periyakgoundar, and S. Gunasekaran, "Magnesium alloys: A review of applications," *Mater. Tehnol.*, vol. 53, no. 6, pp. 881–890, 2019, doi: 10.17222/mit.2019.065.
[62] B. J. Wang, D. K. Xu, J. Sun, and E. H. Han, "Effect of grain structure on the stress corrosion cracking (SCC) behavior of an as-extruded Mg-Zn-Zr alloy," *Corros. Sci.*, vol. 157, no. June, pp. 347–356, 2019, doi: 10.1016/j.corsci.2019.06.017.
[63] S. Payan, Y. Le Petitcorps, J. M. Olive, and H. Saadaoui, "Experimental procedure to analyze the corrosion mechanisms at the carbon/aluminum interface in composite materials," *Compos. Part A Appl. Sci. Manuf.*, vol. 32, no. 3–4, pp. 585–589, 2001, doi: 10.1016/S1359-835X(00)00126-3.
[64] K. Dejun and W. Jinchun, "Salt spray corrosion and electrochemical corrosion properties of anodic oxide film on 7475 aluminum alloy," *J. Alloys Compd.*, vol. 632, pp. 286–290, 2015, doi: 10.1016/j.jallcom.2015.01.175.
[65] N. H. Ononiwu, C. G. Ozoegwu, N. Madushele, O. J. Akinribide, and E. T. Akinlabi, "Mechanical properties, tribology and electrochemical studies of Al/Fly ash/eggshell aluminium matrix composite," *Biointerface Res. Appl. Chem.*, vol. 12, no. 4, pp. 4900–4919, 2022, doi: 10.33263/BRIAC124.49004919.
[66] C. Dupraz, P. T. Visscher, L. K. Baumgartner, and R. P. Reid, "Microbe-mineral interactions: Early carbonate precipitation in a hypersaline lake (Eleuthera Island, Bahamas)," *Sedimentology*, vol. 51, no. 4, pp. 745–765, 2004, doi: 10.1111/j.1365-3091.2004.00649.x.
[67] K. D. Ralston, N. Birbilis, and C. H. J. Davies, "Revealing the relationship between grain size and corrosion rate of metals," *Scr. Mater.*, vol. 63, no. 12, pp. 1201–1204, 2010, doi: 10.1016/j.scriptamat.2010.08.035.
[68] S. O. Akinwamide, B. T. Abe, O. J. Akinribide, B. A. Obadele, and P. A. Olubambi, "Characterization of microstructure, mechanical properties and corrosion response of aluminium-based composites fabricated via casting—a review," *Int. J. Adv. Manuf. Technol.*, vol. 109, no. 3–4, pp. 975–991, 2020, doi: 10.1007/s00170-020-05703-1.